BULLETIN OF THE POLISH ACADEMY OF SCIENCES
TECHNICAL SCIENCES, Vol. 74(4), 2026, Article number: e157565
DOI: 10.24425/bpasts.2026.157565

Enhancing ferro-nanofluid performance in wavy minichannels: Investigating entropy generation and vorticity under magnetic field influence

Anshuman BHADRI[1], **Harvindra SINGH**[1]*, **Pravat RANJAN PATI**[1], **Sunil CHAMOLI**[2], **Chandra KISHORE**[1], **Vishal SHARMA**[3], **Rajkumar CHADGE**[4], and **Mohammad Kanan**[5,6]

[1] Department of Mechanical Engineering, Graphic Era (Deemed to be University), Dehradun, Uttarakhand, India, 248002
[2] Department of Mechanical Engineering, Govind Ballabh Pant Institute of Engineering & Technology, Pauri Garhwal, Uttarakhand, India, 246194
[3] School of Chemical Engineering and Physical Sciences, Lovely Professional University, Phagwara, 144411, India
[4] Department of Mechanical Engineering, Yeshwantrao Chavan College of Engineering, Nagpur, India, 441110
[5] Department of Industrial Engineering, College of Engineering, University of Business and Technology, Jeddah, Saudi Arabia, 21448
[6] Department of Mechanical Engineering, College of Engineering, Zarqa University, Zarqa, Jordan

Abstract. This work examines how channel shape and magnetic field strength influence heat transfer characteristics in magneto-hydrodynamic (MHD) systems. Five different channel geometries were analyzed under magnetic field intensities ranging from 1200 G to 2500 G and Reynolds numbers between 50 and 250. The properties of local flows, vorticity patterns, and entropy formation were examined using numerical simulations. The findings demonstrate that stronger magnetic fields improve heat transfer efficiency, while higher field strengths produce more intricate entropy and vorticity patterns. Heat transfer efficiency is influenced by channel geometry; Case 3 outperforms the others and exhibits the highest levels of vorticity and entropy formation. In all geometries, it was discovered that entropy formation increased with magnetic field strength and decreased with rising Reynolds number. The study also shows that there is a trade-off between flow resistance and heat transfer enhancement, with configurations that generate the highest levels of vorticity and entropy typically exhibiting greater friction factors. Entropy values ranged from 225.67 to 593.26 under different situations and scenarios, with Case 2 showing the highest sensitivity to parameter changes. For a variety of technological applications, these findings provide crucial insights for optimizing MHD-based heat transfer systems and directing the development of efficient thermal management solutions. Heat transmission efficiency is influenced by the form of the channel. While Cases 4 and 5 had more consistent but weaker patterns, Case 3 exhibited the highest vorticity and generated the highest entropy, suggesting higher heat transmission capabilities.

Keywords: wavy channel; ferro nanofluid; magnetic field; entropy; vorticity.

1. INTRODUCTION

Ferro-nanofluids are increasingly being recognized for their effectiveness in thermal management, especially in minichannel applications. These fluids consist of magnetic nanoparticles suspended in a base liquid, enhancing heat transfer efficiency when influenced by external magnetic fields. This feature allows for active manipulation of their flow and thermal properties [1], making them ideal for compact thermal systems [2, 3], such as those used in electronics [4]. Minichannels, characterized by hydraulic diameters ranging from 200 μm to 3 mm, offer an ideal setting for deploying ferro-nanofluids. Their small size increases the surface area-to-volume ratio, which is essential for efficient heat dissipation. As the demand for smaller systems rises, leveraging ferro-nanofluids in these channels could enhance thermal performance, effectively tackling the heat transfer challenges presented by such compact designs [5, 6]. Recent research has underscored the effectiveness of ferro-nanofluids in improving convective heat transfer under the influence of magnetic fields. Jalayeri *et al*. [7] explored the combined impact of a vortex generator and a magnetic field on ferrofluid convective heat transfer in a three-dimensional channel, revealing significant enhancements in performance [8]. Similarly, Boutas *et al.* [9] analyzed the thermal and fluid flow characteristics of ferrofluids in a heat exchanger that featured a magnetic vortex generator, further demonstrating the cooperative advantages of magnetic fields and vortex rise. Furthermore, the use of wavy geometries in minichannels plays a vital role in enhancing heat transfer performance. Wavy channels promote mixing, disrupt boundary layers, and generate secondary flows, all of which contribute to improved heat transfer efficiency. The integration of wavy geometries with ferro-nanofluids and magnetic fields offers a promising avenue for achieving significant enhancements in heat transfer performance. Wavy minichannels present a viable alternative for attaining previously unheard-of degrees of heat transfer improvement when paired with ferro-

*e-mail: harvindrasingh.me@geu.ac.in

Manuscript submitted 2025-05-02, revised 2025-12-18, initially accepted for publication 2026-01-01, published in July 2026.

nanofluids and magnetic fields [10]. The analysis of entropy generation is essential for assessing the efficiency of thermal systems, as it offers important insights into the irreversibilities involved in heat transfer and fluid flow processes [11]. Vorticity is another vital parameter in fluid dynamics, as it significantly contributes to enhancing heat transfer by facilitating mixing and disrupting thermal boundary layers [12]. The creation and regulation of vortices in ferro-nanofluid flows through wavy minichannels can be markedly affected by the application of magnetic fields, providing an additional mechanism for the improvement of heat transfer [13–15]. The impact of magnetic fields on the flow and heat transfer of ferro-nanofluids has been thoroughly examined across different channel configurations [16]. Gürdal *et al*. [17] performed an in-depth review of how nanofluids, magnetic fields, and turbulators influence convective heat transfer in channels, emphasizing the potential for notable enhancements in performance. The utilization of magnetic fields in ferro-nanofluid flows presents distinctive prospects for managing and improving the efficiency of heat transfer. The effects of a magnetic field on the turbulent flow and heat transfer properties of ferronano-fluid flowing in a dimpled tube were examined. Similarly, Altunay *et al.* [18] explored the thermal performance of Fe_3O_4/water nanofluid flowing through a dimpled tube subjected to a nonuniform magnetic field, revealing improved heat transfer properties. The channel geometry is vital for determining the flow and heat transfer characteristics of ferro-nanofluids [19]. In particular, wavy channels demonstrated potential in improving heat transfer due to their capacity to induce secondary flows and enhance mixing [20]. Recent research has examined various facets of ferro-nanofluid flow and heat transfer across different channel configurations. Soleymani *et al.* [21] conducted a numerical study on turbulent flow, heat transfer, and entropy generation of water-based magnetic nanofluid in a tube featuring a hemisphere porous structure under a uniform magnetic field. Their results indicate that the magnetic field can notably enhance the heat transfer performance of ferro-nanofluid. In the case of ferro-nanofluid flow within wavy minichannels subjected to a magnetic field, the significance of entropy generation analysis grows due to intricate interactions among fluid properties, channel geometry, and the external magnetic field. Han *et al.* [22] investigated the impact of a magnetic field on forced convection heat transfer and entropy generation in a microchannel equipped with trapezoidal ribs. Their findings suggest that the magnetic field can improve the heat transfer rate while decreasing entropy generation within the microchannel. The research emphasizes the significance of considering the entropy production and heat transfer enhancement when designing and optimizing thermal systems that employ ferro-nanofluids. The research showed that the application of magnetic fields significantly enhanced heat transfer performance. Similarly, considering different pin-fin forms, Hai *et al.* [23] examined entropy generation in a pin-fin [24] heat sink with Fe3O4 ferrofluid coolant under the effect of a magnetic field. The intricate relationship among ferro-nanofluid characteristics, channel configuration, and magnetic fields demands a thorough knowledge and optimization of heat transfer efficiency. The effect of an applied magnetic field on vortex formation in laminar nanofluid flow was investigated by Ali *et al.* [25], who pointed out the possibility of improved mixing and heat transmission. Abdi *et al.* [26] further demonstrated the complex flow configurations induced by magnetic fields by examining magnetic nanofluid flow in a square cavity subjected to the magnetic field of a wire carrying electric current in a turbulence regime [27]. We believe the current study addresses key research gaps and motivations, as no comprehensive examinations of wavy minichannels in different configurations exist, despite the abundance of studies on the flow and heat transmission of ferro-nanofluid in various channel topologies [28]. Furthermore, the collective behavior of ferro-nanofluids and wavy minichannels in the presence of magnetic fields has not been thoroughly investigated, especially in the context of system optimization [29]. Various wave geometries can change the entropy generation rate and vorticity of ferronanofluids exposed to magnetic field augmentation, affecting their flow and heat transfer behavior [30, 31]. However, there is no evidence that the ferro-nanofluid performance can be enhanced through wavy minichannel augmentation by optimal magnetic field intensity and direction. We expect that an experimental study on entropy generation and vorticity in wavy minichannels using ferro-nanofluid flow under a magnetic field will address these research gaps [32]. The study explores five different wave geometries: a) $y = \sin(x)$, b) $y = \sin(x/2)$, c) $y = \sin(2x)$, d) $y = \sin(3x)$, e) $y = \sin(x/3)$ by performing the ferro-nanofluid flow heat transfer to gain understanding how channel configuration will affect such characteristics. Entropy generation analysis and vorticity investigation will provide a comprehensive understanding. The study seeks to optimize cooling systems on wavy minichannels under magnetic field influence to better understand the underlying phenomenology and the effect of channel configuration on the characteristics of ferro-nanofluid flow heat transfer [33, 34]. The originality of the work lies in its systematic comparison of five different wavy minichannel geometries of various magnetic field strengths – a combination that has not been previously investigated in the literature on ferro-nanofluid heat transfer [35, 36]. Previous research examined individual geometries or magnetic conditions, isolating the effects of wave frequency, magnetic field strength, and ferro-nanofluid properties on entropy generation and vorticity, as well as the conditions resulting in maximum thermo-hydraulic performance. In contrast, this study analyzes the interaction effect of wave frequency, magnetic field strength, and ferro-nanofluid properties simultaneously [37–39].

2. NUMERICAL METHODOLOGY

Two parallel, 40 mm-long plates that formed the 2D wavy microchannel are the subject of the current study. The 4 mm channel width maintains the separation of the two plates from each other. As seen in Fig. 1a, the bottom surface of the channel is wavy to enhance the surface area that is open to heat transfer. The top and bottom surfaces of the microchannel are under isothermal conditions. The Ferro nanofluid, which has a concentration of 2 vol% Fe_3O_4/water, was employed as the cooling fluid in the micro channel. The nanofluid was introduced into this narrow tube at a fixed temperature and intake velocity. The computational flow domain was discretized using a rectangular grid of 80×320 computational nodes, with 80 computational nodes in the vertical direction and 320 nodes in the horizontal direction, to correctly resolve the velocity and heat transfer gradients. Additionally, to increase the precision of the velocity and thermal gradient computations, a bias factor of 4 was applied around the walls. Figure 1b displays the computational domain meshing. In Case 1, a curve driven by the equation $y = \sin(x)$ was used to create the wavy surface. Furthermore, a magnetic field was applied 20 mm from the channelinlet to examine its effects on heat transfer and fluid flow characteristics. Figure 1a shows the computational domain for Case 2, with the position of the magnetic field introduction marked. Figure 1b illustrates the meshing that was utilized to produce precise numerical simulations.

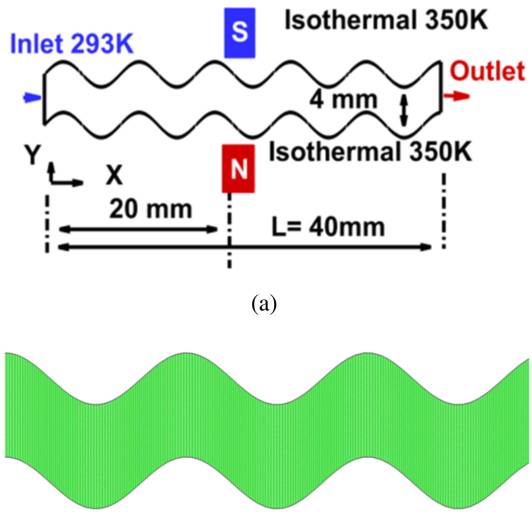

(a)

(b)

Fig. 1. (a) Computational domain used in the present work (Case 1), (b) Meshing of the computational domain

The image is divided into five distinct subparts, labeled (a) through (e), each displaying a unique sinusoidal pattern. In the current research, a total of five different cases were considered, and their details are depicted in Fig. 2. Each case is represented by a different equation-driven curve for the bottom surface of the minichannel. A conventional sine wave, represented by the curve specified by $y = \sin(x)$, is used to show the domain in Fig. 2a. A stretched sine wave, shown by $y = \sin(x/2)$ in Fig. 2b, produces longer, more progressive undulations. Conversely, Fig. 2c shows a compressed wave pattern driven by $y = \sin(2x)$ that oscillates more frequently. The most compact undulations in the series are produced by the additional wave frequency increase of Fig. 2d, using the equation $y = \sin(3x)$. Finally, Fig. 2e displays the wave pattern with the longest wavelength among all the samples, where the most stretched-out wave pattern is defined by $y = \sin(x/3)$. This regular diversity in wave patterns enables an extensive investigation of the effects of different surface geometries on vorticity and entropy within the microchannel.

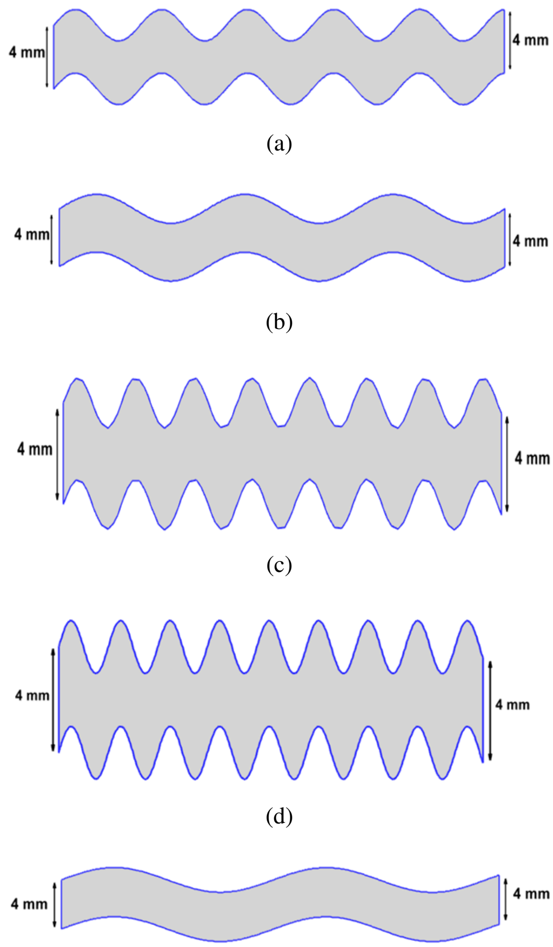

(a)

(b)

(c)

(d)

(e)

Fig. 2. Details of the different computational domains used in the present work: (a) Equation driven curve by $y = \sin(x)$, (b) Equation-driven curve by $y = \sin(x/2)$, (c) Equation-driven curve by $y = \sin(2x)$, (d) Equation driven curve by $y = \sin(3x)$, and (e) Equation driven curve by $y = \sin(x/3)$

2.1. Details of mathematical data reduction

2.1.1. Governing equations

The governing equations for the two-dimensional steady-state homogeneous laminar flow case are the continuity, momentum, and energy equations, with the following format:

Continuity equation:

$$\nabla \cdot (\rho V) = 0. \tag{1}$$

Momentum equation:

$$\nabla \cdot (\rho V V) = -\nabla P + \nabla \cdot (\tau_{ij}) + F_k . \tag{2}$$

The shear stress vector (τ_{ij}) is given by:

$$\tau_{ij} = \mu \left(\frac{\partial v_i}{\partial x_j} + \frac{\partial v_j}{\partial x_i} \right) - \frac{2}{3} \mu \delta_{ij} \left(\frac{\partial v_i}{\partial x_i} \right). \tag{3}$$

Energy equation:

$$\nabla \cdot (\rho V C_p \nabla T) = \nabla \cdot (k \nabla T). \tag{4}$$

The magnetic volume force F_k was added to the momentum equation in equation (2) to account for the effect of the magnetic field on the nanofluid. Since viscous dissipation is negligible in relation to other factors, it is omitted from the analysis.

Using the Maxwell equation, the magnetic flux density $\vec{B}$ was computed as follows:

$$\vec{B} = \mu_0 \left(\vec{M} + \vec{H}\right), \tag{5}$$

where $\vec{M}$ is the magnetization; $\vec{H}$ is the magnetic field intensity; and μ_0 is the permeability of the medium.

The magnetization vector $\vec{M}$ is assumed to be aligned with the magnetic field intensity as:

$$\vec{M} = \chi_m \vec{H}, \tag{6}$$

where χ_m is magnetic susceptibility and is dependent on temperature.

The magnetic volume force is obtained from:

$$F_k = \frac{1}{2}\mu_0 \chi_m (1+\chi_m) \nabla \left(\vec{H}\cdot\vec{H}\right) + \mu_0 \chi_m \vec{H} \left[\left(\vec{H}\cdot\nabla\right)\chi_m\right]. \tag{7}$$

There are two terms on the right side of the equation above. The nonuniform magnetic field is the source of the first dominant term, whereas the magnetic susceptibility gradient of space is the source of the second dominant term. The work assumes that a uniform magnetic force is produced by all four of the magnets. The first term is therefore null. Since temperature affects susceptibility, the second term fluctuates throughout the flow domain. The magnetic volume force and flow direction of the minichannel are hence perpendicular.

Two-dimensional flow vorticity is computed as follows:

$$\omega_z = \nabla u = \frac{\partial v}{\partial x} - \frac{\partial u}{\partial y}. \tag{8}$$

The local total entropy generation rate (S'_{gen}) can be defined as:

$$S'_{\text{gen}} = S'_h + S'_f, \tag{9}$$

where S'_h and S'_f are the local entropy generation rates due to heat transfer and fluid friction, respectively, and are defined as follows:

$$S'_h = \frac{\lambda}{T^2}\left[\left(\frac{\partial T}{\partial X}\right)^2 + \left(\frac{\partial T}{\partial Y}\right)^2 + \left(\frac{\partial T}{\partial Z}\right)^2\right], \tag{10}$$

$$S'_f = \frac{\mu}{T}\left\{2\left[\left(\frac{\partial u_X}{\partial X}\right)^2 + \left(\frac{\partial u_Y}{\partial Y}\right)^2 + \left(\frac{\partial u_Z}{\partial Z}\right)^2\right] + \left(\frac{\partial u_X}{\partial Y} + \frac{\partial u_Y}{\partial X}\right)^2 + \left(\frac{\partial u_X}{\partial Z} + \frac{\partial u_Z}{\partial X}\right)^2 + \left(\frac{\partial u_Y}{\partial Z} + \frac{\partial u_Z}{\partial Y}\right)^2\right\}. \tag{11}$$

The average values of entropy generation rates due to heat transfer (S_{avh}) and fluid friction (S_{avf}) are represented as:

$$S_{\text{avh}} = \frac{\int S'_h \,\mathrm{d}V}{V}, \quad S_{\text{avf}} = \frac{\int S'_f \,\mathrm{d}V}{V}, \tag{12}$$

where V is the volume of the computational domain. Thus, S_{avgen} is given by:

$$S_{\text{avgen}} = S_{\text{avh}} + S_{\text{avf}}. \tag{13}$$

Since the fluid flow is two-dimensional, only domains in the X and Y directions are used in the above equations.

2.2. Boundary conditions and thermophysical properties

The study applies the following boundary conditions: The minichannel bottom wall is heated isothermally to sustain a constant temperature of 350 K, while the top wall is thermally insulated. A ferrofluid with a 293 K initial temperature enters the channel at a steady speed. The channel outlet is set to atmospheric pressure. All fluid-solid interfaces need to adhere to no-slip standards. The physical and magnetic properties of the ferro-nanoparticles used in this investigation are indicated in Table 1.

Table 1
Thermophysical properties of the Fe_3O_4 nanoparticles used as a working fluid

Property	Value
Diameter	20 nm
Density	4950 kg/m^3
Thermal conductivity	7 W/m-K
Specific heat	640 J/Kg-K

Equations that consider both the magnetic nanoparticles and the base fluid (water) are used to calculate the ferrofluid density, specific heat, viscosity, and thermal conductivity:

$$\rho_{nf} = (1-\emptyset)\rho_f + \emptyset\rho_{np}, \tag{14}$$

$$(\rho C_p)_{nf} = (1-\emptyset)(\rho C_p)_f + \emptyset(\rho C_p)_{np}, \tag{15}$$

$$\mu_{nf} = \mu_f (1+2.5\emptyset). \tag{16}$$

where f, np, and nf refer to the base fluid, nanoparticle, and nanofluid, respectively.

Also, the thermal conductivity is calculated by:

$$k_{nf} = k_{\text{Static}} + k_{\text{Brownian}}, \tag{17}$$

$$k_{\text{Static}} = k_f\left[\frac{(k_{np}+2k_f) - 2\emptyset(k_f - k_{np})}{(k_{np}+2k_f) + \emptyset(k_f - k_{np})}\right], \tag{18}$$

$$k_{\text{Brownian}} = 5\times10^4 \beta\emptyset\rho_f C_{p,f}\sqrt{\frac{kT}{\rho_{np}D_{np}}}\, g(\emptyset, T). \tag{19}$$

The Boltzmann constant, k, the nanoparticle concentration, the proportion of liquid volume that goes with a particle, and the modeling function, $g\,(\emptyset, T)$ are all represented in the preceding equations.

$$g = (-6.04\emptyset + 0.4705)\,T + 1722.3\emptyset - 134.63. \tag{20}$$

To improve accuracy, the properties of pure water are expressed as temperature-dependent functions. These include equations for density, specific heat capacity, thermal conductivity, and dynamic viscosity of water, all varying with temperature.

$$\rho_f = 2446 - 20.674T + 0.11576T^2 - 3.12895\times10^{-4}T^3 + 4.0505\times10^{-7}T^4 - 2.0546\times10^{-10}T^5, \tag{21}$$

$$\mu_f = 2.414\times10^{-5}\times10^{\left[\frac{247}{T-140}\right]}, \tag{22}$$

$$k_f = -1.13 + 9.71\times10^{-3}T - 1.31\times10^{-5}T^2. \tag{23}$$

3. RESULTS AND DISCUSSION

3.1. CFD solver settings, grid independent test

Based on the given conditions and assumptions, the current study numerically simulated the problem using the finite volume-based commercial CFD solver ANSYS-Fluent version 2021. The investigation looked at the flow characteristics at extremely low Re = 50, 100, 150, 200, and 250 based on the channel width. As a result, a pressure-velocity coupling viscous laminar model was applied. To achieve accurate numerical findings, a second-order upwind discretization technique was applied to the momentum and energy equations. We assessed our calculations at different grid resolutions to ensure their accuracy and mesh independence. At the channel outlet, we also obtained the nondimensional velocity profile. Figure 3 shows that the outcomes were remarkably similar across all resolutions. To balance computational precision and time, we used a mesh resolution of 80 ×320 (80 vertical nodes and 320 horizontal nodes) for our simulations. The mesh utilized for this study project is displayed in Fig. 1b. Figure 3 shows the asymmetric velocity profile at the outflow resulting from the temperature dependency of the ferrofluid on viscosity. Because viscosity and temperature have an inverse relationship, velocities are higher near the heated bottom wall because of the lower viscosity. As a result, the bottom heated wall experiences the maximum velocity rather than the center. Three different grid sizes were investigated to guarantee grid independence. This research indicated that a mesh size of 80×320 was adequate and chosen for additional study since it provided accurate results while maintaining computational efficiency.

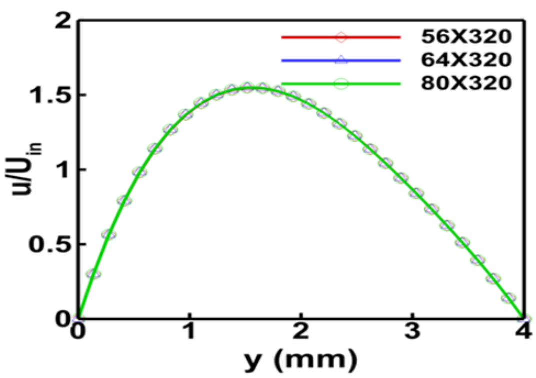

Fig. 3. Nondimensional velocity obtained from different grid generations at channel outlet for Re = 170

3.2. Validation of design model

To verify the validity of the results obtained for different situations, the current results were compared to those produced by [40]. A single magnetic source at $x = 7.5$ mm is applied, and it is seen from Fig. 4 that there is acceptable agreement with the earlier research up to a maximum divergence of 7%.

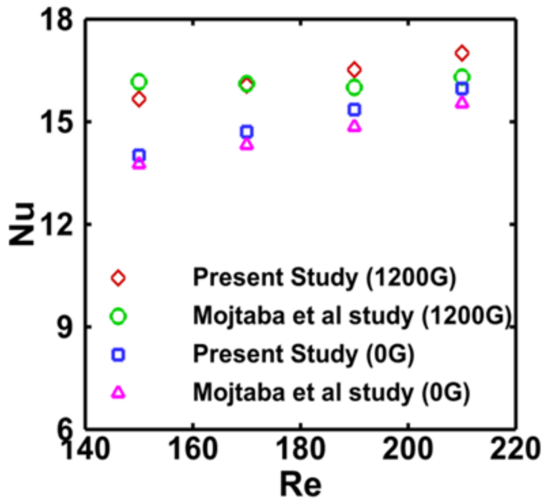

Fig. 4. Numerical results of Nu and Re (a) Validation of numerical study of [41] at B = 0 G and B = 1200 G

3.3. Effects of wavy minichannel on flowing fluid

Figures 5 and 6 display the contours for entropy and vorticity, respectively, which overlapped with streamlines for Case 1 (Figs. 5 and 6) at Reynolds number 100 under different magnetic field strengths ranging from 1200 G to 2500 G, respectively. However, distinct high-velocity zones emerge at the peaks and troughs of the sinusoidal surface when the field strength increases to 2000 G and 2500 G. This phenomenon is believed to be caused by the Lorentz force, which in some locations induces fluid deflection and acceleration. It is produced when the applied magnetic force interacts with a flowing stream. The results in Fig. 5 can be explained by considering the intricate interactions between inertial forces, Lorentz forces, viscous forces, and pressure gradients. Case 1 exhibits a nonuniform entropy distribution with less severe vorticity, suggesting more constant flow conditions and potentially lower total heat transfer rates. Case 1 (a, b, c, and d) suggests a high heat transfer zone with intensive entropy formation, while in Fig. 6, Case 1 (a, b, c, and d) shows stronger vortices and entropy generation, suggesting enhanced heat transfer performance. This observation may be explained

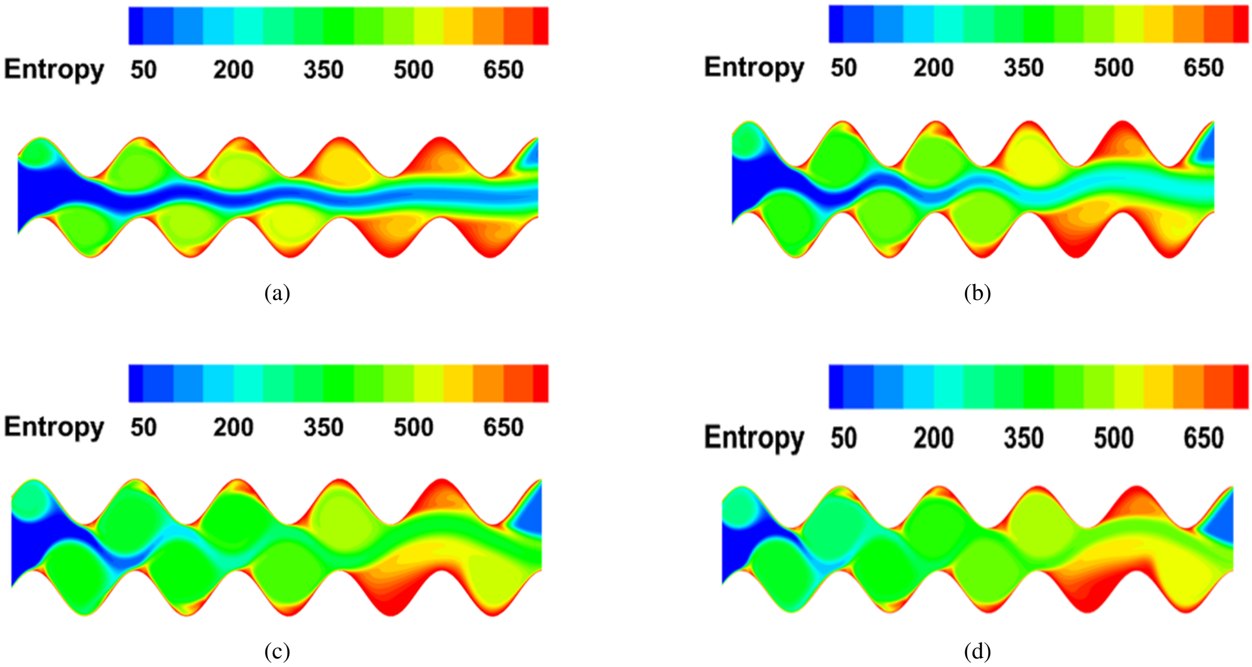

Fig. 5. Entropy contours for Case 1 and Re = 100 at (a) 1200 G, (b) 1500 G, (c) 2000 G, and (d) 2500 G

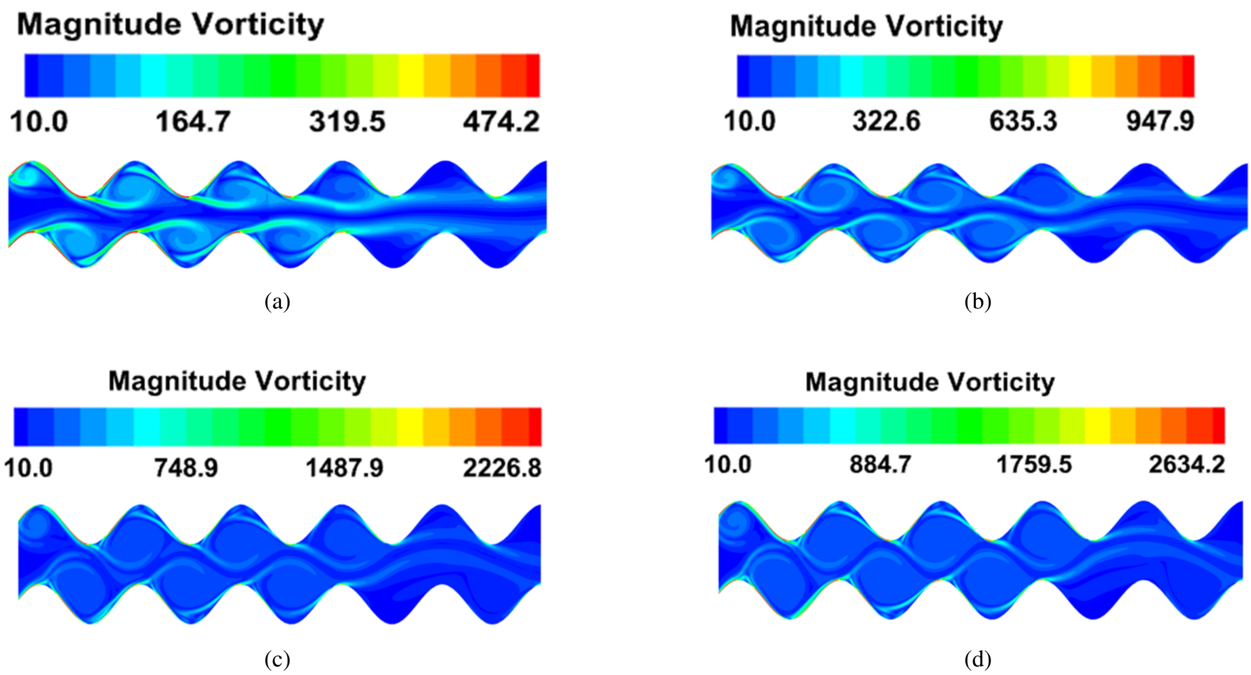

Fig. 6. Vorticity contours for Case 1 and Re = 100 at (a) 1200 G, (b) 1500 G, (c) 2000 G, and (d) 2500 G

by intricate interactions between velocities, viscosities, Lorentz forces, and inertial forces inside the channel. The combined effects include a thinner thermal boundary layer, the appearance of recirculation zones, improved mixing and heat transfer, and accelerated flow areas. These flow properties have important implications for increasing heat transfer in the microchannel because they may result in higher heat transfer rates at stronger magnetic fields. However, the production of recirculation zones may also lead to the development of localized hot spots, which may be detrimental under certain circumstances.

Figures 7 and 8 show significant differences in heat transfer characteristics and flow patterns across different geometries under a constant magnetic field of 1200 Gauss and a Reynolds number of 100.

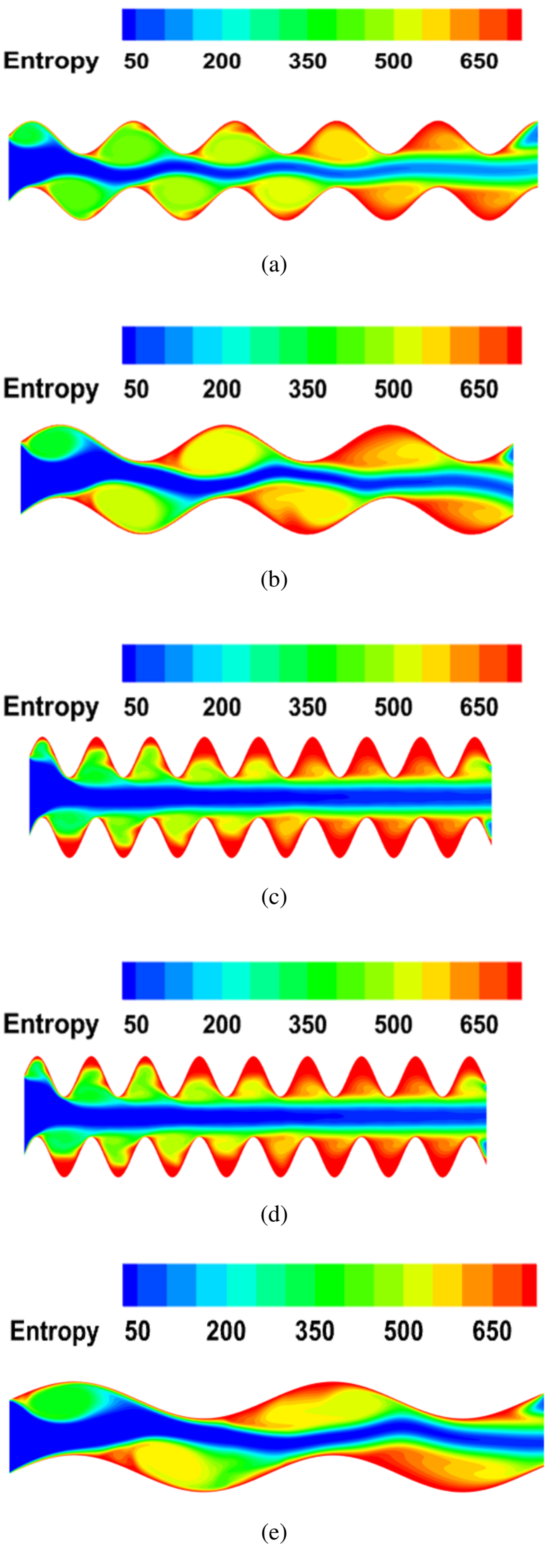

Fig. 7. Entropy contours at 1200 G and Re = 100 for (a) Case 1, (b) Case 2, (c) Case 3, (d) Case 4, and (e) Case 5

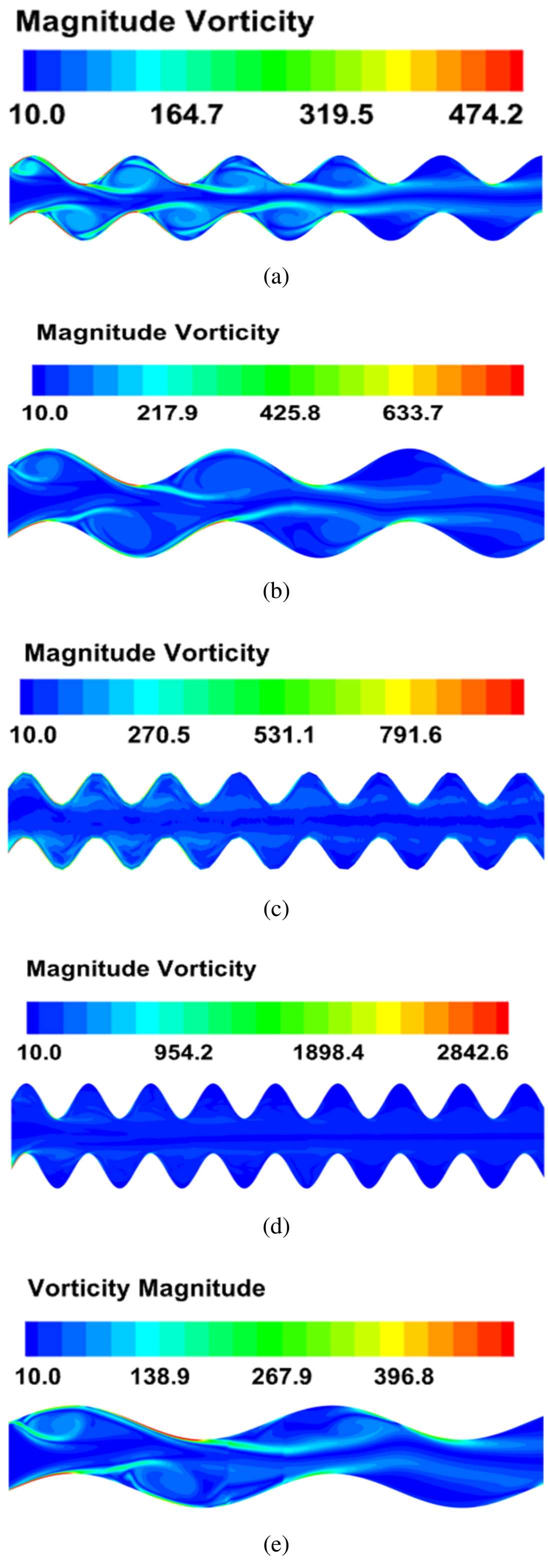

Fig. 8. Vorticity contours at 1200 G and Re = 100 for (a) Case 1, (b) Case 2, (c) Case 3, (d) Case 4, and (e) Case 5

3.4. Effects of magnetic field strength

Figures 9 and 10 depict the intricate connections between flow characteristics, geometric variations, magnetic field strength, and local vorticity distribution along the channel length. The effects of different magnetic field strengths (1200 G, 1500 G, 2000 G, and 2500 G) on local vorticity for Case 1 at Re = 100 are shown in Fig. 9, with distinct results for the upwall (Fig. 9b)

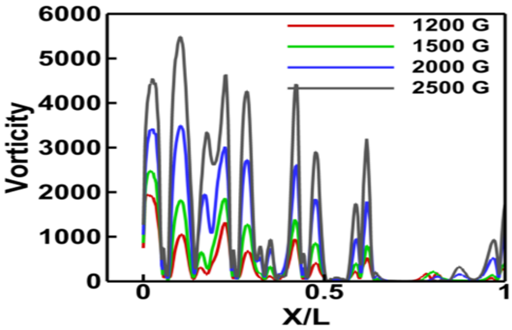

(a)

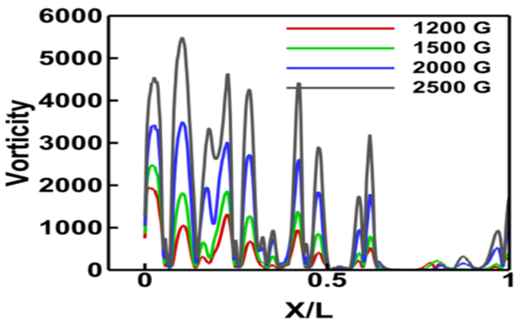

(b)

Fig. 9. Effect of magnetic field on the local vorticity along the channel length for Case 1 at Re = 100 for (a) Downwall, (b) Upwall

and downwall (Fig. 9a). We observe a general amplification of vorticity magnitude along both walls as the magnetic field intensity increases. There are some places where this pattern is remarkably noticeable, which correspond to geometric features or flow separation sites. At greater field strengths, the vorticity peaks sharpen and become more distinct, suggesting stronger localized rotating fluid motion. With stronger magnetic fields, this increase in vorticity could lead to better mixing and higher heat transfer rates. The complicated interplay between the magnetic field and channel geometry is highlighted by the interesting asymmetry observed in the vorticity patterns along the downwall and upwall. This analysis is further extended in Fig. 10, where local vorticity variations are compared for several scenarios (scenarios 1–5) at a given magnetic field strength of 1200 G and Re = 100. The unique vorticity profiles in each scenario highlight how geometric differences have a major effect on flow behavior. The contour plots (Figs. 7–8) supporting the higher heat transfer performance of the configuration are corroborated by Case 3, which displays the largest vorticity peaks along both the downwall (Fig. 10a) and upwall (Fig. 10b). Different instances have different vorticity peak locations, suggesting that different geometry produces different flow topologies and separation points. The vorticity magnitudes in Cases 4 and 5 are milder, indicating softer flow patterns that could provide more consistent, though possibly less intense, heat transmission characteristics. Different downwall and upwall vorticity profiles in each case highlight the asymmetric nature of the flow created by the interaction of geometry and magnetic field. These findings demonstrate how careful geometric design may be used to customize heat transfer performance in MHD systems, since various layouts can significantly change local flow behaviors and, in turn, heat transfer rates under the same magnetic field settings.

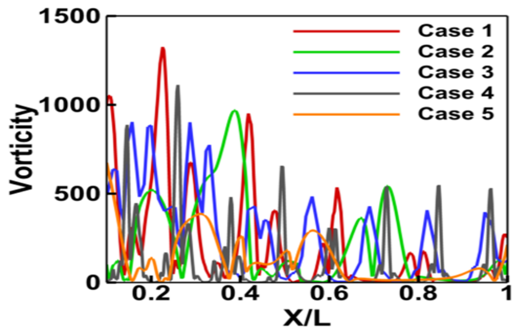

(a)

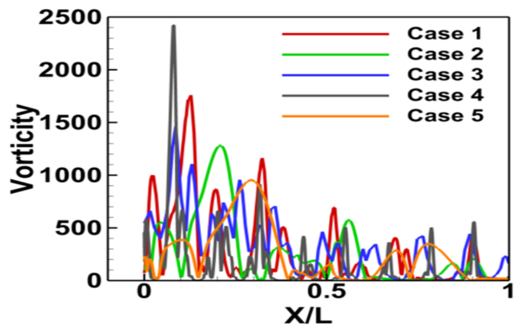

(b)

Fig. 10. Local vorticity variation along the channel length for different Cases at Re = 100 and 1200 G for (a) Downwall, (b) Upwall

3.5. Effects of Reynolds number

For various geometric configurations (Cases 1–5), Figs. 11 and 12 offer vital insights into the entropy behavior of the system under changing Reynolds number (Re) and magnetic field intensity circumstances. The entropy variation with Reynolds number for various magnetic field intensities of each of the five examples is shown in Fig. 11. Entropy exhibits a consistent tendency that increases with greater magnetic field intensities and reduces with increasing Reynolds numbers in all circumstances. Improved fluid mixing and less thermal gradients at greater flow rates are responsible for this inverse relationship between entropy and Re, which results in more effective heat transfer and fewer irreversibilities. On the other hand, larger magnetic fields boost the creation of entropy, probably because of higher Joule heating and more intricate flow patterns that encourage energy dissipation. The fact that these effects differ in strength between the situations emphasizes how important geometry is to the production of entropy. Case 2 appears to be the most sensitive to variations in Re and magnetic field strength, as evidenced by its greatest peak entropy of 593.26 and broadest entropy range of 593.26–2587.74. Case 4, on the other hand, has the narrowest entropy range (513.2–395.2), indicating more reliable perfor-

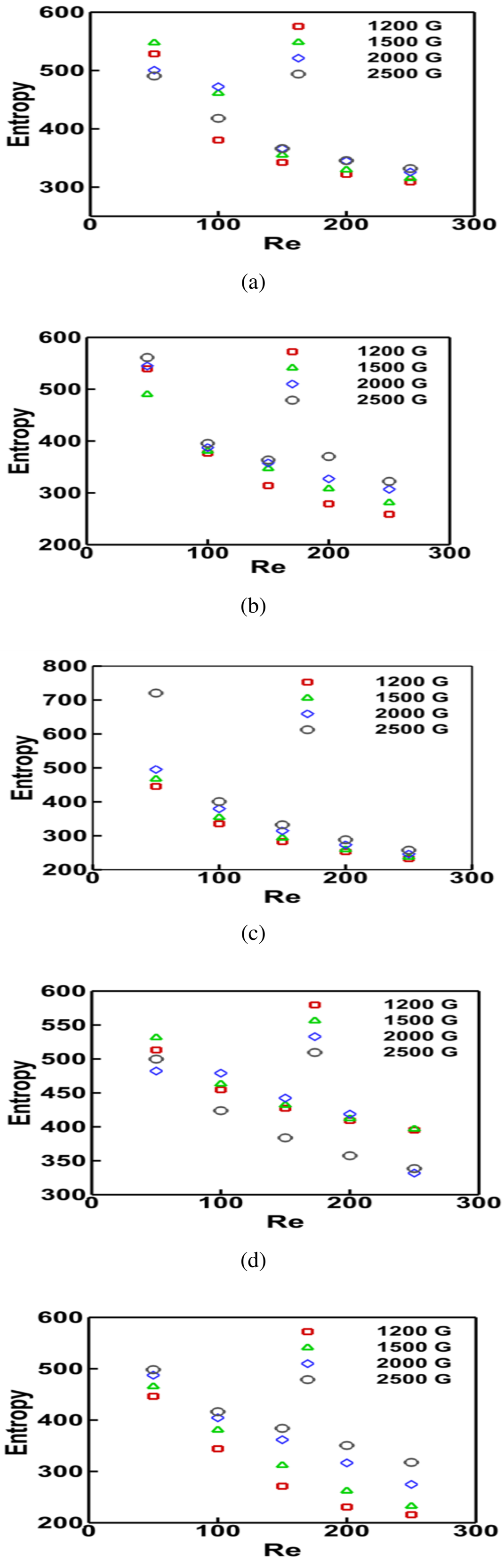

(a)

(b)

(c)

(d)

(e)

Fig. 11. Variation of entropy with Reynolds number for different magnetic fields for (a) Case 1, (b) Case 2, (c) Case 3, (d) Case 4, and (e) Case 5

mance under many circumstances. Case 3 exhibits moderate entropy behavior (445.39–232.7), suggesting a compromise between improved mixing and regulated irreversibilities, despite the significant vorticity features found previously. To facilitate direct comparison across examples, Fig. 12 focuses on entropy variation with Reynolds number at a given magnetic field of 1200 G. In this instance, Case 2 consistently exhibits the maximum entropy for all Reynolds values, supporting the peak value of Fig. 11. This indicates that the geometry of Case 2 may have the highest irreversibilities but may also offer high heat transfer rates. Particularly at higher Reynolds numbers, Cases 3 and 5 show lower entropy values, suggesting that, in these circumstances, they may provide more effective heat transfer with lower irreversibilities. The way that geometry affects the system response to changing flow circumstances is further highlighted by the variable slopes of the entropy-Re curves for the various scenarios in Fig. 12. These findings reveal how geometry, magnetic field intensity, and flow parameters interact to determine the overall system performance. The tendencies discovered offer important insights into optimizing MHD heat transfer systems. These trends indicate that, depending on the operating conditions and whether the goal is to maximize heat transfer or minimize irreversibility, different geometric configurations may be preferable.

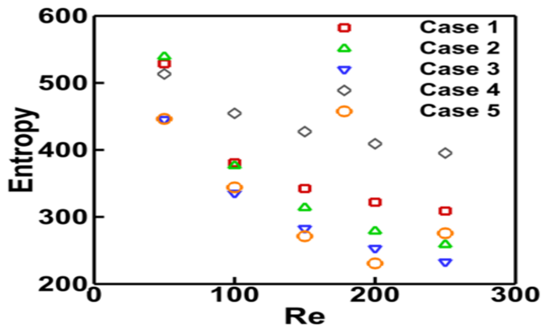

Fig. 12. Entropy variation with Reynolds number at 1200 G for Case 1, Case 2, Case 3, Case 4, Case 5

4. CONCLUSIONS

This work examined the impact of channel shape and magnetic field strength on the properties of heat transmission in magneto-hydrodynamic (MHD) systems. We identified several key findings by analyzing entropy generation, vorticity patterns, and local flow characteristics across various scenarios and conditions:

- Performance in terms of heat transmission is strongly influenced by magnetic field strength.
- The field strength was raised from 1200 G to 2500 G, resulting in more complex entropy and vorticity patterns that suggested higher rates of mixing and heat transmission.
- A key factor in determining heat transfer efficiency is channel shape. Out of the five cases that were examined, Case 3 demonstrated the strongest vorticity and entropy creation, indicating better heat transfer capability. In contrast, Cases 4 and 5 displayed more consistent but weaker patterns.

- Special flow structures arise from the interaction between geometry and magnetic field. Local vorticity analysis reveals asymmetric patterns, and the locations of peak vorticity vary across the cases.
- The creation of entropy exhibits a direct correlation with magnetic field strength and an inverse relationship with Reynolds number. All geometries show the same tendency, with Case 2 exhibiting the greatest sensitivity to these parameters.
- The improvement of heat transmission and flow resistance is mutually exclusive. Higher friction factors are also typically seen in configurations with the highest levels of vorticity and entropy generation, two markers of effective heat transmission.
- Geometry has a major impact on how the system responds to shifting situations. This suggests that by modifying the channel design to satisfy specific operational requirements, MHD heat transfer systems may be optimized. By providing useful data for the design and optimization of MHD-based heat transfer systems, these findings provide a solid foundation for developing more efficient thermal management solutions in a variety of technical applications.

The results are especially relevant to practical applications of mini/micro-scale cooling equipment, electronics thermal control, and lab-on-chip systems and compact heat exchangers, where magnetic fields can be used to actively control heat transfer.

5. LIMITATIONS AND FUTURE WORK

Although the study provides extensive numerical analysis, it has certain limitations. The simulations were performed using a two-dimensional model of laminar flow and assuming a constant field of magnetism, which may not fully capture the three-dimensional and potentially turbulent behavior of ferronanofluids in practical applications. Also, the temperature and magnetic characteristics were idealized, and there was no consideration of the agglomeration of nanoparticles and the effects of field-dependent instability. The future research should therefore provide extensive experimental validation to confirm the numerical trends, especially the predicted vorticity projections, the behavior of entropies, and the maximum levels of the magnetic field. Such efforts would increase the relevance of the results to the advanced cooling methods and microfluidic, magnetically regulated cooling apparatus.

NOMENCLATURE

B	Magnetic field intensity (Gauss)
C_p	Specific heat (J/kg.K)
D	Hydraulic diameter (m)
F_k	Magnetic body force (N)
H	Magnetic field intensity
H	Plate baffle height (m)
W	Width of the plate baffle (m)
h	Convective heat transfer coefficient (W/m^2 K)
K	Thermal conductivity (W/m^{-1} K^{-1})
k	Boltzmann constant
L	2D channel length (m)
M	Magnetization (A m^{-1})
P	Pressure drop (Pa)
q''	Heat flux (W/m^2)
Re	Reynolds number
Nu	Nusselt number
fr	Friction factor
2D	Two-dimensional
T	Temperature (K)
u	Horizontal velocity (m/s)
v	Vertical velocity (m/s)
V	Velocity (m/s)
x, y	Directions
S'_{gen}	Local total entropy generation rate (W/m^3·K)
S'_h	Local entropy generation rate due to heat transfer (W/m^3·K)
S'_f	Local entropy generation rate due to fluid friction (W/m^3·K)
S_{avgen}	Average entropy generation rate (W/m^3·K)
S_{avh}	Average heat transfer entropy generation rate (W/m^3·K)
S_{avf}	Average fluid friction entropy generation rate (W/m^3·K)

Greek Symbols

$\emptyset$	Volume fraction
χ_m	Magnetic susceptibility
χ_o	Differential magnetic susceptibility (0.06)
ρ	Density (kg/m^3)
μ	Dynamic viscosity (N.s/m^2)
μ_0	Permeability of free space ($4\pi\times10^{-7}$N/A^2)
β	Fraction of the liquid volume (k^{-1})
τ	Wall shear stress (Pa)
δ	Kronecker delta

Subscripts

b	Bulk
f	Fluid
nf	Nanofluid
np	Nanoparticle
in	Inlet
w	Wall

REFERENCES

[1] O. Ghaffarpasand, "Effect of alternating magnetic field on unsteady MHD mixed convection and entropy generation of ferro fluid in a linearly heated two-sided cavity," *Sci. Iran.*, vol. 24, no. 3, pp. 1108–1125, 2017, doi: 10.24200/sci.2017.3730.

[2] M. Gürdal, K. Arslan, E. Gedik, and A.A. Minea, "Effects of using nanofluid, applying a magnetic field, and placing turbulators in channels on the convective heat transfer: A comprehensive review," *Renew. Sustain. Energy Rev.*, vol. 162, p. 112453, 2022, doi: 10.1016/j.rser.2022.112453.

[3] M. Tekir, E. Taskesen, B. Aksu, E. Gedik, and K. Arslan, "Comparison of bi-directional multi-wave alternating magnetic field effect on ferromagnetic nanofluid flow in a circular pipe under laminar flow conditions," *Appl. Therm. Eng.*, vol. 179, p. 115624, 2020, doi: 10.1016/j.applthermaleng.2020.115624.

[4] X.H. Sun, M. Massoudi, N. Aubry, Z.H. Chen, and W.T. Wu, "Natural convection and anisotropic heat transfer in a ferronanofluid under magnetic field," *Int. J. Heat Mass Transfer*, vol. 133, pp. 581–595, 2019, doi: 10.1016/j.ijheatmasstransfer. 2018.12.043.

[5] M. Sepehrnia, H. Khorasanizadeh, and M.B. Shafii, "Effect of transverse and parallel magnetic fields on thermal and thermohydraulic performances of ferro-nanofluid flow in trapezoidal microchannel heat sink," *Int. J. Numer. Methods Heat Fluid Flow*, vol. 31, no. 7, pp. 2089–2111, 2021, doi: 10.1108/HFF-08-2020-0523.

[6] W. Cherief *et al.*, "Effect of the magnetic field direction on forced convection heat transfer enhancements in ferrofluids," *Eur. Phys. J. Appl. Phys.*, vol. 71, no. 1, pp. 10901, 2015, doi: 10.1051/epjap/2015140239.

[7] A. Jalayeri, H. Soltanipour, and S. Rezazadeh, "Simultaneous Effects of a Vortex Generator and Magnetic Field on Ferrofluid Convective Heat Transfer in a 3D Channel: First and Second Law Analyses," *AUT J. Mech. Eng.*, vol. 8, no. 2, pp. 85–108, 2024, doi: 10.22221/autjme.8.2.2024.

[8] E.M. Elsaid and M.S. Abdel-wahed, "MHD mixed convection Ferro Fe_3O_4/Cu-hybrid-nanofluid runs in a vertical channel," *Chin. J. Phys.*, vol. 76, pp. 269–282, 2022, doi: 10.1016/j.cjph.2022.04.003.

[9] L. Boutas, M. Marzougui, J. Zinoubi, and S. Gannouni, "Heat and fluid flow characteristics of ferrofluids circulating in a heat exchanger with a magnetic vortex generator," *Heat Transf. Res.*, vol. 55, pp. 1–15, 2024, doi: 10.1615/HeatTransRes.2024.3294225.

[10] M. Gürdal, H.K. Pazarlıoğlu, M. Tekir, K. Arslan, E. Gedik, and E. Taşkesen, "Experimental investigation on thermo-hydraulic performance of ferro-nanofluid flow in a dimpled tube under magnetic field effect," *Exp. Heat Transf.*, vol. 36, no. 3, pp. 312–330, 2023, doi: 10.1080/08916152.2022.2041498.

[11] G. Huminic and A. Huminic, "Entropy Generation Analysis of Hybrid Nanofluids Flow in Ducts with Various Shapes," in *Nanofluids and Their Engineering Applications*, CRC Press, 2019, pp. 77–103, doi: 10.1201/9780429354686.

[12] S. Yekani Motlagh, I. Tolouie, E. Tolouie, and F. Mobadersani, "Ferrofluid Injection and Applied Magnetic Field Influences on the Characteristics of Flow Over a Cylinder," *AUT J. Mech. Eng.*, vol. 7, no. 2, pp. 131–154, 2023, doi: 10.22221/autjme.7.2.2023.

[13] Z. Korei, S. Benissaad, A.J. Chamkha, F. Berrahil, and A. Filali, "Thermohydraulic and second law analyses during the cooling of an electronic device mounted in an open cavity equipped with magnetic nanofluid, magnetic field inducer, and porous media: a two-phase numerical investigation," *Int. Commun. Heat Mass Transf.*, vol. 139, p. 106497, 2022, doi: 10.1016/j.icheatmasstransfer.2022.106497.

[14] J. Mohseni, M. Haratian, and D. Toghraie, "Analysis of the first and second laws of thermodynamics for MHD two-phase natural convection of water/Fe_2O_3 ferro-nanofluids in a 3D baffled enclosure," *Eng. Anal. Bound. Elem.*, vol. 155, pp. 371–400, 2023, doi: 10.1016/j.enganabound.2023.01.013.

[15] Y. Sheikhnejad *et al.*, "Experimental investigation and three-dimensional numerical analysis of ferroconvection through horizontal tube under magnetic field of fixed parallel magnet bars," *J. Heat Transf.*, vol. 139, no. 10, p. 101703, 2017, doi: 10.1115/1.4036581.

[16] M. Bezaatpour, H. Rostamzadeh, J. Bezaatpour, and M. Ebadollahi, "Magnetic-induced nanoparticles and rotary tubes for energetic and exergetic performance improvement of compact heat exchangers," *Powder Technol.*, vol. 377, pp. 396–414, 2021, doi: 10.1016/j.powtec.2021.01.032.

[17] M. Gürdal, H.K. Pazarlıoğlu, M. Tekir, K. Arslan, and E. Gedik, "Numerical investigation on turbulent flow and heat transfer characteristics of ferro-nanofluid flowing in dimpled tube under magnetic field effect," *Appl. Therm. Eng.*, vol. 200, p. 117655, 2022, doi: 10.1016/j.applthermaleng.2021.117655.

[18] F.M. Altunay, H.K. Pazarlıoğlu, M. Gürdal, M. Tekir, K. Arslan, and E. Gedik, "Thermal performance of Fe3O4/water nanofluid flow in a newly designed dimpled tube under the influence of non-uniform magnetic field," *Int. J. Therm. Sci.*, vol. 179, p. 107651, 2022, doi: 10.1016/j.ijthermalsci.2022.107651.

[19] Y. Altunay H. Yan, M. Massoudi, and W.T. Wu, "Effects of anisotropic thermal conductivity and Lorentz force on the flow and heat transfer of a ferro-nanofluid in a magnetic field," *Energies*, vol. 10, no. 7, p. 1065, 2017, doi: 10.3390/en10071065.

[20] M. Bezaatpour and M. Goharkhah, "A magnetic vortex generator for simultaneous heat transfer enhancement and pressure drop reduction in a mini channel," *Heat Transf.*, vol. 49, no. 3, pp. 1192–1213, 2020, doi: 10.1080/08916152.2020.1748784.

[21] P. Soleymani *et al.*, "Numerical investigation on turbulent flow, heat transfer, and entropy generation of water-based magnetic nanofluid flow in a tube with hemisphere porous under a uniform magnetic field," *Int. Commun. Heat Mass Transf.*, vol. 137, p. 106308, 2022, doi: 10.1016/j.icheatmasstransfer.2022.106308.

[22] L. Han *et al.*, "Numerical investigation of magnetic field on forced convection heat transfer and entropy generation in a microchannel with trapezoidal ribs," *Eng. Appl. Comput. Fluid Mech.*, vol. 15, no. 1, pp. 1746–1760, 2021, doi: 10.1080/19942060.2021.1896541.

[23] T. Hai, K. Sharma, A.A. Mohammed, H. Fouad, and W. ElShaai, "The entropy generation analysis of a pin–fin heatsink with Fe_3O_4 ferrofluid coolant and considering four different pin–fin shapes (circular, square, rhumbas, and triangular) in the presence of the magnetic field," *J. Magn. Magn. Mater.*, vol. 580, p. 170904, 2023, doi: 10.1016/j.jmmm.2023.170904.

[24] K. Liu *et al.*, "Numerical simulation method of fork-flow condenser and the influence of fin structure characteristics," *Bull. Pol. Acad. Sci. Tech. Sci.*, vol. 73, p. e154273, 2025, doi: 10.24425/bpasts.2025.154273.

[25] K. Ali, M. Prakash, W. Jamshed, R.W. Ibrahim, S. Ahmad, and Z. Raizah, "Imposed magnetic field impact on vortex generation in the laminar nanofluid flow: A computational approach," *Int. Commun. Heat Mass Transf.*, vol. 139, pp. 106469, 2022, doi: 10.1016/j.icheatmasstransfer.2022.106469.

[26] H. Abdi, S.Y. Motlagh, and H. Soltanipour, "Study of magnetic nanofluid flow in a square cavity under the magnetic field of a wire carrying the electric current in turbulence regime," *Results in Physics*, vol. 18, p. 103224, 2020, doi: 10.1016/j.rinp.2020.103224.

[27] N.S. Akbar, D. Tripathi, Z.H. Khan, and O.A. Bég, "Mathematical model for ciliary-induced transport in MHD flow of Cu-H2O nanofluids with magnetic induction," *Chin. J. Phys.*, vol. 55, no. 3, pp.947–962, 2017, doi: 10.1016/j.cjph.2017.06.004.

[28] M.H. Buschmann, "Critical review of heat transfer experiments in ferrohydrodynamic pipe flow utilising ferronanofluids," *Int. J. Therm. Sci.*, vol. 157, p. 106426, 2020, doi: 10.1016/j.ijthermalsci.2020.106426.

[29] O. Çiçek, A.F. Baytaş, and A.C. Baytaş, "Entropy generation minimization of hybrid nanofluid mixed convection flow in lid-driven square enclosure with heat-generating porous layer on inner walls," *Int. J. Numer. Methods Heat Fluid Flow*, vol. 34, no. 2, pp. 629–665, 2024, doi: 10.1108/HFF08-2023-0591.

[30] S. Li, L. Mao, A.A. Alizadeh, X. Zhang, and S.V. Mousavi, "The application of non-uniform magnetic field for thermal enhancement of the nanofluid flow inside the U-turn pipe at solar collectors," *Sci. Rep.*, vol. 13, no. 1, p. 8471, 2023, doi: 10.1038/s41598-023-34333-1.

[31] M.G. Li, C. Zheng, F. Feng, X. Chen, and W.T. Wu, "Natural convection and anisotropic heat transfer of shear-thinning ferro-nanofluid in partially heated rectangular enclosures under magnetic field," *Therm. Sci. Eng. Prog.*, vol. 25, p. 100992, 2021, doi: 10.1016/j.tsep.2021.100992.

[32] M. Saadat, M. Ghassemi, and M.B. Shafii, "Numerical investigation on the effect of external varying magnetic field on the mixing of ferrofluid with deionized water inside a microchannel for lab-on-chip systems," *Energy Sources A-Recovery Util. Environ. Eff.*, vol. 42, no. 1, pp. 1–13, 2020, doi: 10.1080/15567036.2019.1676828.

[33] E. Taşkesen, M. Tekir, B. Aksu, E. Gedik, and K. Arslan, "The effect of MHD flow on hydrothermal characteristics of ferro-nanofluid in circular pipe," *Exp. Heat Transf.*, vol. 36, no. 5, pp. 617–631, 2023, doi: 10.1080/08916152.2022.2110913.

[34] A.P. Tetuko *et al*., "The effect of magnetic nano-fluids (Fe_3O_4) on the heat transfer enhancement in a pipe with laminar flow," *Heat Mass Transf.*, vol. 56, pp. 65–74, 2020, doi: 10.1007/s00231-019-02669-5.

[35] P. Jalili, M.D Afifi, B. Jalili, A.M. Mirzaei, and D. Ganji, "Numerical study and comparison of two-dimensional ferrofluid flow in semi-porous channel under magnetic field," *Int. J. Eng.*, vol. 36, no. 11, pp. 2087–2101, 2023, doi: 10.1109/IDEA.2023.01299.

[36] B. Sun, Y. Guo, D. Yang, and H. Li, "The effect of constant magnetic field on convective heat transfer of Fe3O4/water magnetic nanofluid in horizontal circular tubes," *Appl. Therm. Eng*., vol. 171, pp. 114920, 2020, doi: 10.1016/j.applthermaleng.2020.114920.

[37] M. Ghadiri, O. Haghani, E. Emam-jomeh, and E. Barati, "Experimental investigation on laminar convective heat transfer of nano ferrofluids under constant and alternating magnetic field," *AUT J. Mech. Eng.*, vol. 5, no. 3, pp. 477–494, 2021, doi: 10.22060/jme.2021.17863.1039.

[38] S. Mei, C. Qi, M. Liu, F. Fan, and L. Liang, "Effects of paralleled magnetic field on thermo-hydraulic performances of Fe_3O_4-water nanofluids in a circular tube," *Int. J. Heat .Mass Transf.*, vol. 134, pp. 707–721, 2019, doi: 10.1016/j.ijheatmasstransfer.2019.01.022.

[39] M. Sheikholeslami and K. Vajravelu, "Nanofluid flow and heat transfer in a cavity with variable magnetic field," *Appl. Math. Comput.*, vol. 298, pp. 272–282, 2017, doi: 10.1016/j.amc.2017.01.042.

[40] S. Yazdani, "Evaluation of water-based Fe3O4 ferrofluid heat transfer in the presence of external electromagnetic field: A review," *J. Mech. Res. Appl.*, vol. 10, no. 4, pp. 1–25, 2020, doi: 10.23940/jmra.10.4.2020.

[41] S. Das, B. Tarafdar, R.N. Jana, and O.D. Makinde, "Magnetic ferro-nanofluid flow in a rotating channel containing Darcian porous medium considering induced magnetic field and Hall currents," *Spec. Top. Rev. Porous Media*, vol. 10, no. 4, pp. 329–348, 2019, doi: 10.1515/stro-20190041.